

Joint Channel Estimation and Turbo Equalization of Single-Carrier Systems over Time-Varying Channels

Yifan Wang, Minhao Zhang, Xingbin Tu, Zhipeng Li, Fengzhong Qu, *Senior Member, IEEE*, Yan Wei

Abstract—Block transmission systems have been proven successful over frequency-selective channels. For time-varying channel such as in high-speed mobile communication and underwater communication, existing equalizers assume that channels over different data frames are independent. However, the real-world channels over different data frames are correlated, thereby indicating potentials for performance improvement. In this paper, we propose a joint channel estimation and equalization/decoding algorithm for a single-carrier system that exploits temporal correlations of channel between transmitted data frames. Leveraging the concept of dynamic compressive sensing, our method can utilize the information of several data frames to achieve better performance. The information not only passes between the channel and symbol, but also the channels over different data frames. Numerical simulations using an extensively validated underwater acoustic model with a time-varying channel establish that the proposed algorithm outperforms the former bilinear generalized approximate message passing equalizer and classic minimum mean square error turbo equalizer in bit error rate and channel estimation normalized mean square error. The algorithm idea we present can also find applications in other bilinear multiple measurements vector compressive sensing problems.

Index Terms—single carrier, bilinear approximate message passing, time-varying channel, joint channel estimation and equalization, turbo equalization, compressive sensing, multiple measurements vector.

I. INTRODUCTION

THE time-varying nature of the channel has always been a challenging problem in communication systems. To mitigate this issue, conventional approach is to partition a large data frame into several smaller data frames and consider the channel to be static while transmitting each small data frame [1]. This approach has been widely adopted in many modulation systems, including single-carrier (SC) and orthogonal frequency division multiplexing (OFDM) system for its effective performance.

In most of the systems that use block transmission, the channels of different time frames are supposed to be independent [2]. However, in practice, since the channel is generated by the physical surroundings, there must be some relationships

Yifan Wang, Minhao Zhang, Xingbin Tu and Zhipeng Li are with the Key Laboratory of Ocean Observation-Imaging Testbed of Zhejiang Province, Zhejiang University, Zhoushan 316021, China, and also with the Engineering Research Center of Oceanic Sensing Technology and Equipment, Ministry of Education, Zhoushan 316021, China (e-mail: wyfssgn@zju.edu.cn; z_mh@zju.edu.cn; xbtu@zju.edu.cn; joeli@zju.edu.cn).

Fengzhong Qu and Yan Wei are with the Key Laboratory of Ocean Observation-Imaging Testbed of Zhejiang Province, Zhejiang University, Zhoushan 316021, China, also with the Engineering Research Center of Oceanic Sensing Technology and Equipment, Ministry of Education Zhoushan 316021, China, and also with Hainan Institute of Zhejiang University, Sanya 572025, China (e-mail: jimqufz@zju.edu.cn; redwine447@zju.edu.cn).

between the channels across the time domain that can be exploited to enhance the systems' performance.

A. Joint channel estimation and equalization

Equalization of channels has always been a significant topic in wireless communication. In general, there are two main techniques in wireless communication that address this issue. One is based on channel estimation (CE) which assumes that the receiver is aware of the channel, e.g., minimum mean square error (MMSE) equalization [3] and frequency domain equalization with generalized approximate message passing (FD-GAMP) [4]. The alternative technique employs directive equalizers that use adaptive algorithms, such as least mean square (LMS), recursive least squares (RLS) or their variants, and principles such as minimum symbol error rate (MSER) rather than MMSE principle, for example, adaptive minimal symbol error rate (AMSER) [5] and improved proportionate normalized minimum symbol error rate equalizer (IPNMSE) [6].

CE-based equalizers provide excellent performance. However, in low signal-to-noise ratio (SNR) scenarios, the reliability of channel estimated by the pilot degrades significantly, and the symbol detection in the equalization phase is affected as well. One possible way to calibrate the channel estimation result would be to use the symbol that comes out of the turbo equalizer [7]. However, the channel estimation is a hard, rather than soft estimation, which could result in the error being magnified throughout the process. Regarding adaptive equalizer, they need a long pilot to converge their tap coefficient, and equalizers that use decision feedback structures might experience performance degradation due to error propagation in low SNR [8].

The joint channel estimation and equalization/decoding method is an innovative equalizer. One recent work that leverages the bilinear generalized approximate message passing (BiGAMP) [9] designs a joint equalizer with a full soft-input and soft-output (SISO) structure [10]. The term "full" here means that not only is the symbol a soft-input and soft-output as in a normal turbo equalizer, but also the channel. The estimation results of the channel have their expectations and variances, which means every tap has its own degree of confidence. In algorithms based on message passing, this prevents errors from being amplified by some erroneously estimated channel taps similar to what the low-density parity check (LDPC) decoder does to the input log-likelihood ratios (LLRs) with small values [11]. Therefore, it can outperform traditional CE-based algorithms in both the bit error rate

(BER) and normalized mean square error (NMSE) of the channel. It has shown significant advantage in burst data transmission scenarios [12] compared to adaptive equalizers and CE-based equalizers. However, this algorithm fails to address the time-varying nature of the channel.

B. Dynamic Compressive Sensing

To take advantage of the time-varying nature of the channel, we adopt the concept of dynamic compressive sensing. In reality signals are usually correlated in the time domain, such as video reconstruction [13] and time-varying channel estimation [14]. A variety of compressive sensing (CS) algorithms have been proposed that leverage measurements over different time frames. One group of approaches is based on convex relaxation, such as group-fused Lasso, dynamic Lasso [15] and modified-CS algorithm [16]. The alternative group is based on Bayesian theory, such as T-MSBL [17] and DCS-AMP [18]. SBL-based algorithms outperform the others in estimating signals that are not sparse, or whose sensing matrix columns have significant correlation [19], while AMP-based techniques converge quickly and have minimal computational complexity. In our communication problem model, the columns of the sensing matrix are not highly correlated, so DCS-AMP will not suffer significant performance degradation. Moreover, it is also belongs to the family of approximate message passing algorithm, similar to BiGAMP, making it easier to combine its benefits with the BiGAMP algorithm for solving dynamic compressive sensing (DCS) issues.

C. Turbo Equalization

As a fully soft equalizer, the turbo equalization is an indispensable part. Turbo equalization is a successful application of Bayesian theory and sum-product algorithm (SPA) [20]. In turbo equalization, both the expectation and variance are provided to the decoder for decoding to calculate extrinsic LLRs. Then the LLRs output from the decoder will be regarded as *a priori* probabilities and resent to the equalizer. The messaging exchange eventually makes the final LLRs converge close to the *a posteriori* probability, although they will never attain true *a posteriori* probability. This has been elucidated by belief propagation (BP) [21] and SPA [11].

When the channel impulse response (CIR) is known to the receiver, a trellis-based equalizer [22] [23] can be used to build a turbo equalizer, but the complexity of the equalizer will increase exponentially with the number of CIR taps. In practical scenarios, must equalizers can be modified to a turbo equalizer by utilizing LLRs from decoder as *a priori* when estimating the symbols. To our knowledge, the message that passes within most turbo equalizers are limited between the equalizer and decoder. A BiGAMP-based equalizer can transmit messages between the channel estimator, equalizer and decoder, but only within a single time frame. In this paper, we will break this limitation.

D. Contributions

In this paper, we propose a new algorithm, referred to as DCS-BiGAMP, which introduce the dynamic compressive

sensing joint channel estimation and equalization/decoding (DCS-JCED) algorithm inspired by BiGAMP and DCS-AMP. Expectation maximization (EM) and LDPC decoder are respectively used for updating the *a priori* probability of the channel and symbols. We demonstrate that the message in the equalizer can not only be passed between the (SISO) equalizer and decoder but also the channel estimator in multiple time domain. The proposed equalizer i) exploits the correlation between multiple channels across different time frames, ii) achieves a lower NMSE for channel estimates and a better (BER) result compared to the existing equalizer based solely on BiGAMP, and iii) is well suited for sparse channels. These claims are supported by numerical simulations with an extensively validated underwater acousti (UWA) channel generated by [24].

The scope of this work differs from that of the original equalizer based on BiGAMP [10] [12] which only considers time-invariant channels and assumes independence between channels in each frame. Here, we utilize the time-varying characteristics across multiple data frames.

The remainder of the paper is organized as follows. Section II presents the SC block transmission system and the channel model. In Section III, we present the proposed DCS-BiGAMP joint channel estimation and equalization. We also describe how to integrate it with an LDPC decoder to create a turbo equalizer. In Section IV, we present benchmark and performance analysis of our equalizers with existing equalizer. Finally, we draw the conclusions in Section V.

The notations used in this paper are as follows. Boldface uppercase \mathbf{A} denotes a matrix and boldface lowercase \mathbf{a} denotes a vector. a_i represents the i^{th} element of \mathbf{a} . $\mathbf{Z}^{(i)}$ refers to the i^{th} slice along the second dimension of a three-dimensional tensor. \mathbf{I}_M denotes the $M \times M$ identity matrix, $\mathbf{O}_{M,N}$ denotes the $M \times N$ all-zero matrix, and $\mathbf{1}_M$ denotes the $M \times 1$ all-one vector. \mathbf{F}_N denotes the $N \times N$ unitary discrete Fourier transform (DFT) matrix, and $\mathbf{F}_N^{1:L}$ is the matrix that includes columns 1 through L of \mathbf{F}_N . $\mathbf{a}[k]$ denotes the vector involved in the model of the k^{th} data frame. $(\cdot)^T$ represents the transpose, $(\cdot)^H$ represents the conjugate transpose, and $(\cdot)^*$ represents the conjugate. \odot and $|\cdot|^{\odot 2}$ represent element-wise multiplication and squared absolute value, respectively. $\mu_{a \rightarrow b}$ represents the message passed from node a to node b . $\text{Ber}(\cdot)$ denotes Bernoulli distribution, $\mathcal{CN}(\cdot)$ denotes complex Gaussian distribution.

II. SYSTEMS MODEL

In this section we depict the frame structure of the SC block transmission system and the received signal model expressed using tensor and vector multiplication. We also show how to use the Gaussian-Markov process to establish a simple time-varying channel model.

A. Frame structure

In the SC block transmission system, each baseband frame takes the form of

$$\mathbf{x} = [\mathbf{x}_p^T, \mathbf{x}_c^T, \mathbf{x}_g^T]^T, \quad (1)$$

where $\mathbf{x}_g = \mathbf{0}_{N_g \times 1}$ is the zero guard sequence with N_g being greater than the channel length L and $\mathbf{x}_p \in \mathbb{R}^{N_p \times 1}$ is the pilot sequence modulated by binary phase shift keying (BPSK). In this paper, we choose the M-sequence as the pilot sequence. $\mathbf{x}_c \in \mathcal{A}^{N_{cd} \times 1}$ is the information sequence, where $\mathcal{A} \triangleq [\alpha_1, \alpha_2, \dots, \alpha_{2Q}]$ denotes the symbol alphabet, e.g. $Q = 2$ indicates QAM modulation.

The message sequence \mathbf{x}_c carries N_b information bits $b = [b_1, b_2, \dots, b_{N_b}]^T$ where $b_n \in \{0, 1\}$ and $n \in [1, N_b]$. These bits are first passed through an interleaver and then encoded by an encoder to generate a coded bit stream consisting of $N_{code} = N_b/R$ bits, where R is the code rate of the encoder. The encoded bits are then divided into N_{cd} subgroups, i.e. $\mathbf{c} = [\mathbf{c}_1^T, \mathbf{c}_2^T, \dots, \mathbf{c}_{N_{cd}}^T]^T$, where $N_{cd} = N_{code}/Q$ and $\mathbf{c}_n = [c_{n,1}, c_{n,2}, \dots, c_{n,Q}]^T$. Then \mathbf{c} is mapped to \mathbf{x}_c .

The received signal of the k^{th} data frame in the baseband is expressed as

$$y_n[k] = \sum_{l=1}^L x_{n-l+1}[k]h_l[k] + w_n[k], \quad n = 1, 2, \dots, M, \quad (2)$$

where $h_l[k]$ is the l^{th} tap of CIR in the time frame when the k^{th} data frame is transmitted. Since we use a quasi-static channel, h_l will not change within one frame. w_n is an additive zero-mean white Gaussian noise sequence with a variance of σ_w . We rewrite the received signal in matrix form as follows:

$$\begin{aligned} \mathbf{y}[k] &= \mathbf{z}[k] + \mathbf{w}[k] \\ &= \sum_{l=1}^L h_l[k] \mathbf{Z}^{(l)} \mathbf{x}[k] + \mathbf{w}[k], \end{aligned} \quad (3)$$

where

$$\mathbf{Z}^{(l)} = \begin{bmatrix} \mathbf{0}_{(l-1) \times (M-l+1)} & \mathbf{0}_{(l-1) \times (l-1)} \\ \mathbf{I}_{M-l+1} & \mathbf{0}_{(M-l+1) \times (l-1)} \end{bmatrix}, \quad (4)$$

and $N_c = M = N_{cd} + N_p + N_g$. We also define $\mathbf{z}^{(i,j)}$ as the j^{th} column of $\mathbf{Z}^{(i)}$.

B. Channel model

The common underwater acoustic time-varying multipath CIR is modeled by the transfer function [24] [25]

$$H(f, t) = \sum_p h_p(t_n) \gamma_p(f, t) e^{-j2\pi f \tau_p(t)}, \quad (5)$$

where $\gamma_p(f, t)$ with $p = 0, 1, \dots$ represents the scattering coefficient, $\tau_p(t) = \tau_{p0} - a_p t$ represents the time-varying path delay according to the random Doppler scaling factors a_p , and $h_p(t_n)$ represents the path gain. The scattering coefficients are modeled as complex-valued Gaussian processes, and their statistical properties' correlation in time and frequency are determined by the variance $\sigma_{\delta p}^2$ and Doppler bandwidth $B_{\delta p}$ of the intra-path delays.

The detailed physical model is extremely complicated, so we use a simplified model [18] to describe it. The time-varying channel can be decomposed into two parts: support and amplitude. Recall that we assume the CIR is static in

one data frame but time-varying across multiple frames. The channel of the k^{th} time frame $\mathbf{h}[k]$ is represented by

$$\mathbf{h}[k] = \mathbf{s}[k] \cdot \boldsymbol{\theta}[k], \quad (6)$$

where $\mathbf{s}[k] \in \{0, 1\}^{L \times 1}$ represents the support of $\mathbf{h}[k]$ and $\boldsymbol{\theta} \in \mathbb{C}^{L \times 1}$ represents the amplitude of $\mathbf{h}[k]$. Both the support and amplitude change over time.

We describe the support using two transition probabilities $p_{01} = p(s_i[k] = 0 | s_i[k-1] = 1)$ and $p_{10} = p(s_i[k] = 1 | s_i[k-1] = 0)$, which determine a first-order Markov chain for $s_i[k]$ where $i = 1, \dots, L$, and each chain is independent. The marginal probability of $p(s_i[k] = 1)$ is λ and we assume that the Markov chain is in steady-state. By solving

$$\begin{bmatrix} p_{00} & p_{01} \\ p_{10} & p_{11} \end{bmatrix} \begin{bmatrix} 1 - \lambda \\ \lambda \end{bmatrix} = \begin{bmatrix} 1 - \lambda \\ \lambda \end{bmatrix}, \quad (7)$$

we can obtain $p_{10} = \lambda p_{01} / (1 - \lambda)$, which implies p_{01} itself can determine how the chain evolves over time. A small p_{01} generates a static process, while a greater p_{01} generates a more dynamic process. Note that $1/p_{01}$ indicates the average length of a continuous sequence of ones.

For the amplitude, we assume that $\lambda_i[k]$ is independent for $i = 1, \dots, L$, and we use a Gauss-Markov process to describe it, i.e.,

$$\theta_i[k] = (1 - \varrho)(\theta_i[k-1] - \zeta) + \varrho w_i[k] + \zeta, \quad (8)$$

where $\zeta \in \mathbb{C}$ is the mean of the process, and $w_i[k] \sim \mathcal{C}(0, \rho)$ is a Gaussian driving process. $\varrho \in [0, 1]$ represents the degree of correlation. If $\varrho = 1$, the entire process is a simple Gaussian random process, and if $\varrho = 0$, the process becomes a static sequence where all elements are equal to $\theta_i[0]$. Note that (8) implies the conditional and marginal probability of $\theta_i[k]$, i.e.,

$$p(\theta_i[k] | \theta_i[k-1]) = \mathcal{CN}(\theta_i[k] | (1 - \varrho)(\theta_i[k-1] - \zeta) + \zeta, \varrho^2 \rho) \quad (9)$$

$$p(\theta_i[k]) = \mathcal{CN}(\zeta, \sigma^2), \quad (10)$$

where $\sigma^2 = \frac{\varrho \rho}{2 - \varrho}$.

We combine the previously described support and amplitude processes to provide the *a priori* probability for CIR of each frame as a Bernoulli-Gaussian distribution

$$p(h_i[k]) = (1 - \lambda) \delta(h_i[k]) + \lambda \mathcal{CN}(\zeta, \sigma^2). \quad (11)$$

The parameter λ controls the sparsity level of the channel. Although this model is straightforward, it captures the most significant features of the channel, namely its time-varying and sparsity nature, with parameters denoted by $\mathbf{q} = [p_{01}, \lambda, \zeta, \varrho, \rho]$.

III. FULLY SOFT EQUALIZER IN TIME-VARYING CHANNEL

In this section, we present our joint channel estimation and equalization/decoding algorithm based on the proposed algorithm DCS-BiGAMP, and show how to perform turbo equalization. We also show how to adjust the coefficients of the *a priori* probabilities using the EM tuning algorithm.

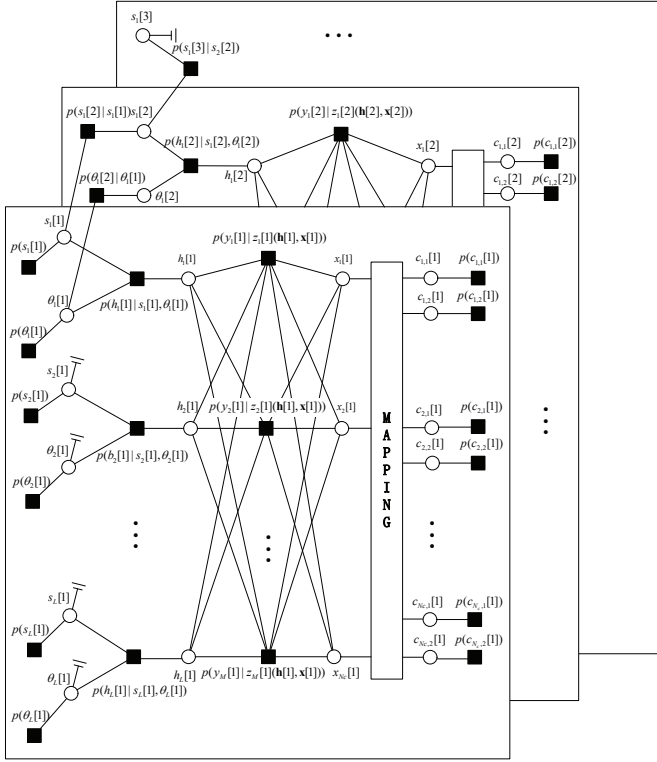


Fig. 1. Factor graph for DCS-BiGAMP equalizer.

A. Message Passing in Bilinear Dynamic compressive sensing

Our fully soft-input and soft-output equalizer estimates both the mean and variance of the channel and symbol through the *a posteriori* probability $p(\mathbf{h}[k]|\mathbf{y}[k], \mathbf{q})$ and $p(\mathbf{x}[k]|\mathbf{y}[k], \mathbf{d})$. They are simplified to be complex Gaussian distributions in the approximate message passing theory, where \mathbf{d} represents the *a priori* probability returned from the decoder. The first step involves constructing to construct the total probability formula:

$$\begin{aligned}
 & p(\bar{\mathbf{y}}, \bar{\mathbf{h}}, \bar{\mathbf{x}}, \bar{\boldsymbol{\theta}}, \bar{\mathbf{s}}) \\
 &= \prod_{k=1}^K p(\mathbf{y}[k]|\mathbf{z}[k](\mathbf{h}[k], \mathbf{x}[k]))p(\mathbf{h}[k]|\mathbf{s}[k], \boldsymbol{\theta}[k])p(\mathbf{x}[k]) \\
 &= \prod_{k=1}^K \left[\prod_{m=1}^M p(y_m[k]|z_m[k](\mathbf{h}[k], \mathbf{x}[k])) \prod_{i=1}^L p(h_i[k]|s_i[k], \theta_i[k]) \right. \\
 & \quad \left. \times p(s_i[k]|s_i[k-1])p(\theta_i[k]|\theta_i[k-1]) \prod_{j=1}^{N_c} p(x_j[k]) \right], \tag{12}
 \end{aligned}$$

where $\bar{\mathbf{y}} \triangleq \{\mathbf{y}[k]\}_{k=1}^T$, and similar for $\bar{\mathbf{h}}, \bar{\mathbf{x}}, \bar{\boldsymbol{\theta}}, \bar{\mathbf{s}}$.

Using the total probability formula, we can create a corresponding factor graph, as shown in Fig. 1. Each hollow circle represents a variable node, and each solid block represents a factor node. A variable node stands for a variable, while a factor nodes stands for a probability density function (PDF). The edge connecting a variable node and a factor node denotes that the variable is an argument of the PDF. Here the factor graph for each frame is placed independently in a plane. The correlation of the channel is expressed by connecting $\theta_i[k]$ and

TABLE I
FACTORS AND THE CORRESPONDING PDFS

factor	PDF
$g_m^k(\mathbf{h}[k], \mathbf{x}[k])$	$p(y_m[k] z_m[k](\mathbf{h}[k], \mathbf{x}[k]))$
$f_i^k(h_i[k], s_i[k], \theta_i[k])$	$p(h_i[k] s_i[k], \theta_i[k])$
$q_i^k(s_i[k])$	$p(s_i[k])$
$q_i^k(s_i[k], s_i[k-1])$	$p(s_i[k] s_i[k-1])$
$v_i^k(\theta_i[k])$	$p(\theta_i[k])$
$v_i^k(\theta_i[k], \theta_i[k-1])$	$p(\theta_i[k] \theta_i[k-1])$
$d_j^k(x_j[k])$	$p(x_j[k])$

$\theta_i[k-1]$ with $p(\theta_i[k]|\theta_i[k-1])$, and by connecting $s_i[k]$ and $s_i[k-1]$ with $p(s_i[k]|s_i[k-1])$. To make our graph concise, we only include the connection between two time frames for $s_i[k]$ and $\theta_i[k]$ when $k = 1, 2, 3$. For a single time frame, we only show connections for $h_i[k]$ when $i = 1, 2, L$, $x_j[k]$, when $j = 1, 2, N_c$, $p(y_m[k]|z_m[k](\mathbf{h}[1], \mathbf{x}[1]))$ when $m = 1, 2, M$.

The *a posteriori* probabilities of $p(\mathbf{h}[k]|\mathbf{y}[k], \mathbf{q})$ and $p(\mathbf{x}[k]|\mathbf{y}[k], \mathbf{d}[k])$ are computed using the BiGAMP algorithm, which is a simplified algorithm based on SPA. Here, $\mathbf{d}[k]$ denotes the *a priori* information of the k^{th} data frame feedback from the decoder. Although obtaining the true *a posteriori* probabilities using SPA requires that no loop is allowed in the factor graph [26], which is not achievable in our factor graph in Fig. 1, we can still obtain an approximate *a posteriori* probability. This has been successfully demonstrated in many applications of SPA, such as LDPC code [27], GAMP [28], VAMP [29] and turbo equalization [20].

To simplify the expression in writing the message, we need to rename the factor nodes instead of referring to them as PDF since they represent corresponding relationships as listed in Table I, before a detailed description of the DCS-BiGAMP algorithm.

The DCS-BiGAMP framework is structurally similar to DCS-AMP, which also utilizes the SPA algorithm to propagate messages between different temporal frames. These messages are used to update the “local prior” which refers to the *a priori* probability of $h_i[k]$: $p(h_i[k]|s_i[k], \theta_i[k])$. The “local prior” enables the original BiGAMP to function within one time frame. The process can be divided into four stages: *into*, *within*, *out* and *across*. In the *into* stage, variable nodes $s_i[k]$ and $\theta_i[k]$ gather messages from factor nodes q_i^k , q_i^{k-1} , v_i^k and v_i^{k-1} , and generate new messages that are then forwarded to f_i^k as the “local prior” of $h_i[k]$. In the *within* stage, original BiGAMP algorithm is performed to calculate the extrinsic expectation and variance of $h_i[k]$ and $x_i[k]$. We denote \hat{q}_i^k and $\mu_i^q[k]$ as the extrinsic expectation and variance of $h_i[k]$, respectively, while the corresponding values for $x_j[k]$ are \hat{r}_j^k and $\mu_j^r[k]$. In the *out* stage, messages from f_i^k to $\theta_i[k]$ and $s_i[k]$ are updated using the extrinsic information returned from the *within* stage. Finally, $s_i[k]$ and $\theta_i[k]$ pass the messages they gathered from factor nodes q_i^k and v_i^k to update $s_i[k-1]$ and $\theta_i[k-1]$. A comprehensive explanation of these four stages will be presented later. Note that the framework can run in either serial or parallel mode. In serial mode, the *into* stage is performed only for $k = 1$, followed by the *within* and *out* stages. The *across* stage only updates $s_i[2]$ and $\theta_i[2]$, and then the same flow path is performed for $k = 2, 3, \dots, K$.

In parallel mode, all frames (i.e. $k = 1, 2, \dots, K$) run the *into*, *within*, and *out* stages simultaneously. In the *across* stage, the update of $s_i[k]$ and $\theta_i[k]$ is still conducted serially. Only a brief explanation of the forward propagation process is presented here. The backward propagation is extremely similar to this, with the exception that the *across* stage need to be modified.

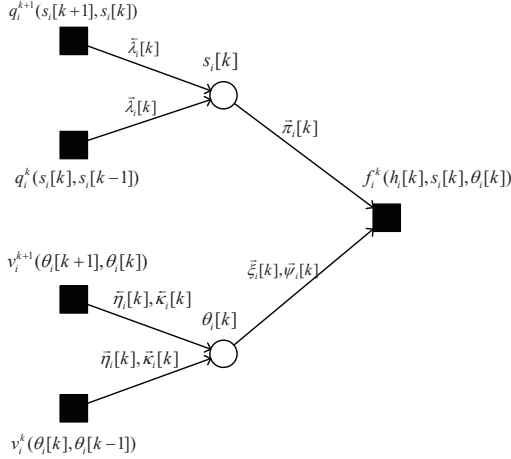


Fig. 2. Factor graph for *into* stage.

In the *into* stage as shown in Fig 2, we need to calculate two messages, $\mu_{s_i[k] \rightarrow f_i^k}$ and $\mu_{\theta_i[k] \rightarrow f_i^k}$ using SPA. For message from $s_i[k]$ to f_i^k , we have

$$\begin{aligned} \mu_{s_i[k] \rightarrow f_i^k} &= \mu_{q_i^{k+1} \rightarrow s_i[k]} \mu_{q_i^k \rightarrow s_i[k]} \\ &= \text{Ber}(s_i[k] | \overleftarrow{\lambda}_i[k]) \text{Ber}(s_i[k] | \overrightarrow{\lambda}_i[k]) \\ &= (1 - \overleftarrow{\lambda}_i[k])(1 - \overrightarrow{\lambda}_i[k])(1 - s_i[k]) \\ &\quad + \overleftarrow{\lambda}_i[k] \overrightarrow{\lambda}_i[k] s_i[k] \\ &= (1 - \overrightarrow{\pi}_i[k])(1 - s_i[k]) + \overrightarrow{\pi}_i[k] s_i[k], \end{aligned} \quad (13)$$

where

$$\overrightarrow{\pi}_i[k] = \frac{\overleftarrow{\lambda}_i[k] \overrightarrow{\lambda}_i[k]}{(1 - \overleftarrow{\lambda}_i[k])(1 - \overrightarrow{\lambda}_i[k]) + \overleftarrow{\lambda}_i[k] \overrightarrow{\lambda}_i[k]}. \quad (14)$$

Similarly, for message from $\theta_i[k]$ to f_i^k , we have

$$\begin{aligned} \mu_{\theta_i[k] \rightarrow f_i^k} &= \mu_{v_i^{k+1} \rightarrow \theta_i[k]} \mu_{v_i^k \rightarrow \theta_i[k]} \\ &= \mathcal{CN}(\theta_i[k] | \overleftarrow{\eta}_i[k], \overleftarrow{\kappa}_i[k]) \mathcal{CN}(\theta_i[k] | \overrightarrow{\eta}_i[k], \overrightarrow{\kappa}_i[k]) \\ &= \mathcal{CN}(\theta_i[k] | \overrightarrow{\xi}_i[k], \overrightarrow{\psi}_i[k]), \end{aligned} \quad (15)$$

where

$$\overrightarrow{\psi}_i[k] = \left(\frac{1}{\overleftarrow{\kappa}_i[k]} + \frac{1}{\overrightarrow{\kappa}_i[k]} \right)^{-1} \quad (16)$$

$$\overrightarrow{\xi}_i[k] = \overrightarrow{\psi}_i[k] \left(\frac{\overleftarrow{\eta}_i[k]}{\overleftarrow{\kappa}_i[k]} + \frac{\overrightarrow{\eta}_i[k]}{\overrightarrow{\kappa}_i[k]} \right) \quad (17)$$

according to the Gaussian multiplication rule [30].

During the first forward propagation, $\overleftarrow{\lambda}$, $\overleftarrow{\kappa}$ and $\overleftarrow{\eta}$ are not updated by the *across* stage of backward propagation, so we initialize them to 0.5, $+\infty$ and 0, respectively. In the last frame, i.e., $k = K$, where there are no q^{K+1} and v^{K+1} , we

have $\overrightarrow{\pi}[K] = \overleftarrow{\lambda}[K]$, $\overrightarrow{\psi}[K] = \overleftarrow{\kappa}[K]$ and $\overrightarrow{\xi}[K] = \overleftarrow{\eta}[K]$. Furthermore, $\overleftarrow{\lambda}[1]$ is initialized with λ and $(\overleftarrow{\eta}_i[1], \overleftarrow{\kappa}_i[1])$ is initialized with (ζ, σ^2) .

The *within* stage is almost the BiGAMP algorithm itself [9]. Nonetheless, the original version only provides the *a posteriori* information of the symbol at the end of the iteration, whereas a SISO equalizer requires extrinsic information. Therefore, we modify the order of the original algorithm. The initial input becomes extrinsic variance and expectation instead of *a posteriori* ones, and so is the final output. In the following, we provide a description of the modified algorithm. One can find the frequency domain version in the Appendix. The first step of the *within* phase is to calculate the *a posteriori* information using the local prior generated in the *into* stage and the LLRs feedback from the decoder. The *a posteriori* probability of the channel is

$$\begin{aligned} p(h_i[k] | \mathbf{y}[k], \overrightarrow{\pi}_i[k], \overrightarrow{\xi}_i[k], \overrightarrow{\psi}_i[k]) \\ = (1 - \pi_i[k]) \delta(h_i[k]) + \pi_i[k] \mathcal{CN}(h_i[k] | \gamma_i[k], \nu_i[k]), \end{aligned} \quad (18)$$

where

$$\nu_i[k] = \left(\frac{1}{\mu_i^q[k]} + \frac{1}{\overrightarrow{\psi}_i[k]} \right)^{-1} \quad (19)$$

$$\gamma_i[k] = \nu_i[k] \left(\frac{\hat{q}_i[k]}{\mu_i^q[k]} + \frac{\overrightarrow{\xi}_i[k]}{\overrightarrow{\psi}_i[k]} \right) \quad (20)$$

$$\pi_i[k] = \frac{1}{1 + \frac{(1 - \overrightarrow{\pi}_i[k]) \mathcal{CN}(0 | \hat{q}_i[k], \mu_i^q[k])}{\overrightarrow{\pi}_i[k] \mathcal{CN}(0 | \overrightarrow{\xi}_i[k] - \hat{q}_i[k], \overrightarrow{\psi}_i[k] + \mu_i^q[k])}}. \quad (21)$$

Hence, the *a posteriori* expectation and variance of $h_i[k]$ are expressed as

$$\hat{h}_i[k] = \pi_i[k] \gamma_i[k] \quad (22)$$

$$\mu_i^h[k] = \pi_i[k] (\gamma_i[k]^2 + \nu_i[k]^2 - \pi_i[k] \gamma_i[k]^2). \quad (23)$$

Similarly, the *a posteriori* probability of the symbol is

$$\begin{aligned} p(x_j[k] = \alpha_n | \mathbf{y}[k], \mathbf{d}[k]) \\ \propto p_{\text{apr}}(x_j[k] = \alpha_n) \mathcal{CN}(x_j[k] | \hat{r}_j[k], \mu_j^x[k]), \end{aligned} \quad (24)$$

and

$$p_{\text{apr}}(x_j[k] = \alpha_n) = \prod_q p(c_{j,q} = \chi_{n,q}). \quad (25)$$

Here, $\chi_{n,q}$ represents the q^{th} bit of the constellation α_n , and

$$p(c_{j,q}) = \frac{\exp((-1)^{c_{j,q}} L_{\text{apr}}(c_{j,q})/2)}{\exp(L_{\text{apr}}(c_{j,q})/2) + \exp(-L_{\text{apr}}(c_{j,q})/2)}, \quad (26)$$

where $L_{\text{apr}}(c_{j,q})$ denotes the *a priori* LLR of bit $c_{j,q}$ coming from the decoder. Consequently, the *a posteriori* expectation and variance of $x_j[k]$ can be expressed as

$$\hat{x}_j[k] = \sum_n p(x_j[k] = \alpha_n | \mathbf{y}[k], \mathbf{d}[k]) \alpha_n \quad (27)$$

$$\mu_j^x[k] = \sum_n p(x_j[k] = \alpha_n | \mathbf{y}[k], \mathbf{d}[k]) |\alpha_n - \hat{x}_j[k]|^2. \quad (28)$$

The second step of the *within* stage is to calculate the conditional expectation and variance of $\mathbf{z}[k]$, namely $p(\mathbf{z}[k]|\mathbf{h}[k], \mathbf{x}[k])$

$$\hat{p}_m[k] = \hat{z}_m^{(*,*)}[k] - \hat{s}_m[k]\bar{\nu}_m^p[k] \quad (29)$$

$$\nu_m^p[k] = \bar{\nu}_m^p[k] + \sum_{i=1}^L \sum_{j=1}^{N_c} \mu_i^h[k] \mu_j^x[k] \left| z_m^{(i,j)} \right|^2, \quad (30)$$

where

$$\hat{z}_m^{(*,*)}[k] = \sum_{i=1}^L \sum_{j=1}^{N_c} \hat{h}_i[k] \hat{x}_j[k] z_m^{(i,j)} \quad (31)$$

$$\bar{\nu}_m^p[k] = \sum_{j=1}^{N_c} \mu_j^x[k] \left| \hat{z}_m^{(*,*)}[k] \right|^2 + \sum_{i=1}^L \mu_i^h[k] \left| \hat{z}_m^{(i,*)}[k] \right|^2 \quad (32)$$

$$\hat{z}_m^{(i,*)}[k] = \sum_{j=1}^{N_c} \hat{x}_j[k] z_m^{(i,j)} \quad (33)$$

$$\hat{z}_m^{(*,j)}[k] = \sum_{i=1}^L \hat{h}_i[k] z_m^{(i,j)}. \quad (34)$$

We omit the definition of \hat{s}_m which is the first derivative used to simplify the message in the inference process of BiGAMP [9] here. It will be defined in the next step of BiGAMP and used during iteration in this step.

In the third step, the *a posteriori* expectation and variance of $\mathbf{z}[k]$ are computed. The Gaussian distribution parameters of $p(\mathbf{z}[k]|\mathbf{h}[k], \mathbf{x}[k])$ are provided in the previous step, and $p(\mathbf{y}[k]|\mathbf{z}[k]) \sim \mathcal{CN}(\mathbf{y}[k]|\mathbf{z}[k], \sigma_w \mathbf{I})$ in our model, so the variance and expectation of $p(\mathbf{z}[k]|\mathbf{y}[k], \mathbf{h}[k], \mathbf{x}[k])$ are

$$\mu_m^z[k] = \left(\frac{1}{\nu_m^p[k]} + \frac{1}{\sigma_w} \right)^{-1} \quad (35)$$

$$\hat{z}_m[k] = \mu_m^z[k] \left(\frac{y_m[k]}{\sigma_w} + \frac{\hat{p}_m[k]}{\nu_m^p[k]} \right). \quad (36)$$

In the fourth step, the parameters $\hat{s}_m[k]$ and $\mu_m^s[k]$, which are used for Taylor expansion in BiGAMP, are calculated as follows

$$\hat{s}_m[k] = \frac{\hat{z}_m[k] - \hat{p}_m[k]}{\nu_m^p[k]} \quad (37)$$

$$\mu_m^s[k] = \left(1 - \frac{\mu_m^z[k]}{\nu_m^p[k]} \right) \frac{1}{\nu_m^p[k]}. \quad (38)$$

The final step of the *within* stage is to estimate the extrinsic parameters of $\mathbf{h}[k]$ and $\mathbf{x}[k]$. $p_{\text{ext}}(\mathbf{h}[k]) \sim \mathcal{CN}(\mathbf{h}[k]|\hat{\mathbf{q}}[k], \boldsymbol{\mu}^q[k])$ and its coefficients are given by

$$\mu_i^q[k] = \left(\sum_{m=1}^M \nu_m^s[k] \left| \hat{z}_m^{(i,*)}[k] \right|^2 \right)^{-1} \quad (39)$$

$$\hat{q}_i[k] = \hat{h}_i[k] + \mu_i^q[k] \sum_{m=1}^M \hat{s}_m[k] \hat{z}_m^{(i,*)}[k]^* - \mu_i^q[k] \hat{h}_i[k] \sum_{m=1}^M \mu_m^s[k] \sum_{j=1}^{N_c} \mu_j^x[k] \left| z_m^{(i,j)} \right|^2. \quad (40)$$

$p_{\text{ext}}(\mathbf{x}[k]) \sim \mathcal{CN}(\mathbf{x}[k]|\hat{\mathbf{r}}[k], \boldsymbol{\mu}^r[k])$ and its coefficients are computed similarly by

$$\mu_j^r[k] = \left(\sum_{m=1}^M \nu_m^s[k] \left| \hat{z}_m^{(*,j)}[k] \right|^2 \right)^{-1} \quad (41)$$

$$\hat{r}_j[k] = \hat{x}_j[k] + \mu_j^r[k] \sum_{m=1}^M \hat{s}_m[k] \hat{z}_m^{(*,j)}[k] - \mu_j^r[k] \hat{x}_j[k] \sum_{m=1}^M \mu_m^s[k] \sum_{i=1}^L \mu_i^h[k] \left| z_m^{(i,j)} \right|^2. \quad (42)$$

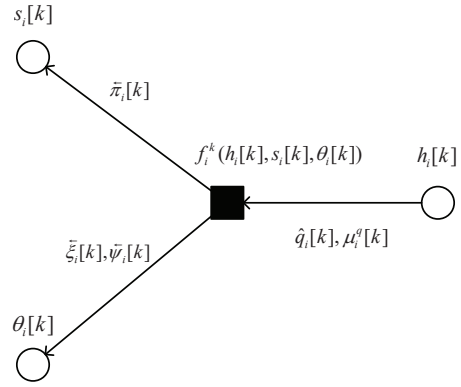


Fig. 3. Factor graph for *out* stage.

The entire *within* stage is completed here. The subsequent extrinsic Gaussian distribution parameters of \mathbf{h} are used in the *out* stage to transfer the information to the other frame, while the corresponding parameters of \mathbf{x} are used to calculate the extrinsic LLRs and send them to the decoder.

The *out* stage is illustrated in Fig 3. The message from $f_i^k(h_i[k], s_i[k], \theta_i[k])$ to $s_i[k]$ can be computed directly by:

$$\begin{aligned} \mu_{f_i^k \rightarrow s_i[k]} &= \int p(h_i[k]|s_i[k], \theta_i[k]) \mu_{h_i[k] \rightarrow f_i^k} \mu_{\theta_i[k] \rightarrow f_i^k} dh_i[k] d\theta_i[k] \\ &= \int \delta(h_i[k] - s_i[k] \theta_i[k]) \mathcal{CN}(\theta_i[k]|\vec{\xi}_i[k], \vec{\psi}_i[k]) \\ &\quad \times \mathcal{CN}(h_i[k]|\hat{q}_i[k], \mu_i^q[k]) dh_i[k] d\theta_i[k] \\ &= \int \mathcal{CN}(\theta_i[k]|\vec{\xi}_i[k], \vec{\psi}_i[k]) \\ &\quad \times \mathcal{CN}(s_i[k] \theta_i[k]|\hat{q}_i[k], \mu_i^q[k]) d\theta_i[k]. \end{aligned} \quad (43)$$

Note that $s_i[k]$ can only be 0 or 1, and thus (43) can be further simplified as

$$\begin{aligned} \mu_{f_i^k \rightarrow s_i[k]} &= \mathcal{CN}(0|\hat{q}_i[k], \mu_i^q[k]) (1 - s_i[k]) \\ &\quad + \mathcal{CN}(0|\hat{q}_i[k] - \vec{\xi}_i[k], \mu_i^q[k] + \vec{\psi}_i[k]) s_i[k] \\ &= (1 - \leftarrow_{\pi_i[k]}) (1 - s_i[k]) + \leftarrow_{\pi_i[k] s_i[k]}, \end{aligned} \quad (44)$$

where

$$\leftarrow_{\pi_i[k]} = \frac{\mathcal{CN}(m_1, \sigma_1)}{\mathcal{CN}(m_1, \sigma_1) + \mathcal{CN}(0|\hat{q}_i[k], \mu_i^q[k])} \quad (45)$$

$$\begin{cases} m_1 = \hat{q}_i[k] - \vec{\xi}_i[k] \\ \sigma_1 = \mu_i^q[k] + \vec{\psi}_i[k]. \end{cases} \quad (46)$$

Updating the message from $f_i^k(h_i[k], s_i[k], \theta_i[k])$ to $\theta_i[k]$ is quite complicated. Direct computation will return a Gaussian mixture distribution with two components, which is unacceptable in message passing algorithms since Gaussian mixture distributions of multiple elements will be generated in later steps during the iteration process. Fortunately, an approach that employs Taylor expansion to approximate the Gaussian mixture distribution with a single Gaussian distribution. $\mathcal{CN}(\theta_i[k] | \overleftarrow{\xi}_i[k], \overleftarrow{\psi}_i[k])$ is provided in [31]. Additionally, an approximation using threshold is proposed in [18]. We choose the former for using in DCS-BiGAMP since the threshold approximation may lead to numerical instability in numerical simulation. To complete our algorithm, we include the approximation flow path in Table II.

TABLE II
APPROXIMATION OF GAUSSIAN MIXTURE DISTRIBUTION

Intermediate variable	
$\Omega(\overleftarrow{\pi}_i[k]) \triangleq \frac{\epsilon^2 \overleftarrow{\pi}_i[k]}{(1 - \overleftarrow{\pi}_i[k] + \epsilon^2 \overleftarrow{\pi}_i[k])}, \epsilon \rightarrow 0$	(A1)
$a \triangleq \epsilon^2(1 - \Omega(\overleftarrow{\pi}_i[k]))$	(A2)
$\bar{a} \triangleq \Omega(\overleftarrow{\pi}_i[k])$	(A3)
$b \triangleq \frac{\epsilon^2}{\mu_i^q[k]} (1 - \frac{1}{\epsilon})\hat{q}_i[k] ^2$	(A4)
$\sigma_r \triangleq -\frac{2\epsilon^2}{\mu_i^q[k]} (1 - \frac{1}{\epsilon})\Re\{\hat{q}_i[k]\}$	(A5)
$\sigma_i \triangleq -\frac{2\epsilon^2}{\mu_i^q[k]} (1 - \frac{1}{\epsilon})\Im\{\hat{q}_i[k]\}$	(A6)
Compute outputs	
$\overleftarrow{\psi}_i[k] = \frac{(a^2 e^{-b} + a\bar{a} + \bar{a}^2 e^b)\mu_i^q[k]}{\epsilon^2 a^2 e^{-b} + a\bar{a}(\epsilon^2 + 1 - \frac{1}{2}\mu_i^q[k]\sigma_r^2) + \bar{a}^2 e^b}$	(A7)
$\overleftarrow{\xi}_i^r[k] = \Re\{\hat{q}_i[k]\} - \frac{1}{2}\overleftarrow{\psi}_i[k] \frac{-ae^{-b}\sigma_r}{ae^{-b} + \bar{a}}$	(A8)
$\overleftarrow{\xi}_i^i[k] = \Im\{\hat{q}_i[k]\} - \frac{1}{2}\overleftarrow{\psi}_i[k] \frac{-ae^{-b}\sigma_i}{ae^{-b} + \bar{a}}$	(A9)
$\overleftarrow{\xi}_i[k] = \overleftarrow{\xi}_i^r[k] + j\overleftarrow{\xi}_i^i[k]$	(A10)

Following the *out* stage, we have the *across* stage as shown in Fig 4. Here, the soft information of the channel concerning joint channel estimation and equalization of one frame is passed to the next frame, enabling us to utilize information across multiple data frames. The messages from q^{k+1} to $s_i[k+1]$ and from v_i^{k+1} to $\theta_i[k+1]$ are updated and used to provide a more confident local prior for the next frame. These two messages can be computed using SPA directly.

To update $\mu_{q_i^{k+1} \rightarrow s_i[k+1]}, \mu_{s_i[k] \rightarrow q_i^{k+1}}$ is first computed as

$$\begin{aligned} \mu_{s_i[k] \rightarrow q_i^{k+1}} &\propto \mu_{f_i^k \rightarrow s_i[k]} \mu_{q_i^k \rightarrow s_i[k]} \\ &= (1 - \overleftarrow{\pi}_i[k])(1 - \overleftarrow{\lambda}_i[k])(1 - s_i[k]) \\ &\quad + \overleftarrow{\pi}_i[k] \overleftarrow{\lambda}_i[k] s_i[k], \end{aligned} \quad (47)$$

and the final result is

$$\begin{aligned} \mu_{q_i^{k+1} \rightarrow s_i[k+1]} &\propto \sum_{s_i[k]} p(s_i[k+1] | s_i[k]) \mu_{s_i[k] \rightarrow q_i^{k+1}} \\ &= p(s_i[k+1] | s_i[k] = 0)(1 - \overleftarrow{\pi}_i[k])(1 - \overleftarrow{\lambda}_i[k]) \\ &\quad + p(s_i[k+1] | s_i[k] = 1) \overleftarrow{\pi}_i[k] \overleftarrow{\lambda}_i[k] \\ &= (1 - \overleftarrow{\lambda}_i[k+1])(1 - s_i[k+1]) + \overleftarrow{\lambda}_i[k+1] s_i[k+1], \end{aligned} \quad (48)$$

where

$$\overleftarrow{\lambda}_i[k+1] = \frac{p_{11} \overleftarrow{\pi}_i[k] \overleftarrow{\lambda}_i[k] + p_{01}(1 - \overleftarrow{\pi}_i[k])(1 - \overleftarrow{\lambda}_i[k])}{(1 - \overleftarrow{\pi}_i[k])(1 - \overleftarrow{\lambda}_i[k]) + \overleftarrow{\pi}_i[k] \overleftarrow{\lambda}_i[k]}. \quad (49)$$

$\mu_{v_i^{k+1} \rightarrow \theta_i[k+1]}$ can be derived using a similar approach. Specifically,

$$\begin{aligned} \mu_{\theta_i[k] \rightarrow v_i^{k+1}} &= \mu_{v_i^k \rightarrow \theta_i[k]} \mu_{f_i^k \rightarrow \theta_i[k]} \\ &= \mathcal{CN}(\theta_i[k] | c, C), \end{aligned} \quad (50)$$

where $C = \frac{\overleftarrow{\kappa}_i[k] \overleftarrow{\psi}_i[k]}{\overleftarrow{\kappa}_i[k] + \overleftarrow{\psi}_i[k]}$, $c = \frac{\overleftarrow{\eta}_i[k] \overleftarrow{\psi}_i[k] + \overleftarrow{\xi}_i[k] \overleftarrow{\kappa}_i[k]}{\overleftarrow{\kappa}_i[k] + \overleftarrow{\psi}_i[k]}$ and

$$\begin{aligned} \mu_{v_i^{k+1} \rightarrow \theta_i[k+1]} &= \int p(\theta_i[k+1] | \theta_i[k]) \mu_{\theta_i[k] \rightarrow v_i^{k+1}} d\theta_i[k] \\ &= \int \frac{1}{1-\varrho} \mathcal{CN}\left(\theta_i[k+1] - \zeta, \frac{\varrho^2 \rho}{(1-\varrho)^2}\right) \\ &\quad \times \mathcal{CN}(\theta_i[k] | c, C) d\theta_i[k] \\ &= \frac{1}{1-\varrho} \mathcal{CN}\left(0 | \frac{\theta_i[k+1] - \zeta}{1-\varrho} + \zeta - c, \frac{\varrho^2 \rho}{(1-\varrho)^2} + C\right) \\ &= \mathcal{CN}(\theta_i[k+1] | \overleftarrow{\eta}_i[k+1], \overleftarrow{\kappa}_i[k+1]), \end{aligned} \quad (51)$$

with

$$\overleftarrow{\eta}_i[k+1] = (1-\varrho)c + \varrho\zeta \quad (52)$$

$$\overleftarrow{\kappa}_i[k+1] = (1-\varrho)^2 C + \varrho^2 \rho. \quad (53)$$

The DCS-BiGAMP joint channel estimation and equalization algorithm is now complete. The output *a posteriori* coefficients of the channel are then used to update the *a priori* coefficients through the EM algorithm, and the output extrinsic coefficients of symbols are used to generate extrinsic LLRs.

B. Extrinsic Log-likelihood Rate

AMP-based estimation algorithms have a significant advantage that they can provide extrinsic information during the iteration process. In contrast, traditional algorithms like LMMSE [3] [32], LMS and RLS [33] require modification in order to compute extrinsic LLRs and take into account the *a priori* LLRs. As shown in Section III-A substituting the Gaussian *a priori* distribution with a discrete distribution allows for the natural incorporation of a priori LLRs. Additionally, computing extrinsic LLRs with the output of DCS-BiGAMP is also straightforward, which is presented as follows.

In the *within* stage of DCS-BiGAMP, we have already computed the extrinsic expectation $\hat{r}_j[k]$ and variance $\mu_j^r[k]$, which is exactly what we need. The extrinsic LLR of the q^{th} bit belonging to symbol $x_j[k]$ can be expressed as ¹

$$\begin{aligned} L_{\text{ext}}(c_j, q) &= \frac{\sum_{\alpha_n \in \mathcal{A}_q^0} \exp\left(\frac{|\alpha_n - \hat{r}_j|^2}{\mu_j^r}\right) \prod_{q' \setminus q} p(c_j, q' = \chi_{n, q'})}{\sum_{\alpha_n \in \mathcal{A}_q^1} \exp\left(\frac{|\alpha_n - \hat{r}_j|^2}{\mu_j^r}\right) \prod_{q' \setminus q} p(c_j, q' = \chi_{n, q'})} \\ &= \ln \frac{\sum_{\alpha_n \in \mathcal{A}_q^0} \exp\left(\frac{|\alpha_n - \hat{r}_j|^2}{\mu_j^r}\right) \sum_{q' \setminus q} (-1)^{\chi_{n, q'}} \frac{L_{\text{apr}}(c_j, q')}{2}}{\sum_{\alpha_n \in \mathcal{A}_q^1} \exp\left(\frac{|\alpha_n - \hat{r}_j|^2}{\mu_j^r}\right) \sum_{q' \setminus q} (-1)^{\chi_{n, q'}} \frac{L_{\text{apr}}(c_j, q')}{2}}, \end{aligned} \quad (54)$$

¹We omit the parameter k here, which denotes the index of data frame, to simplify the expression.

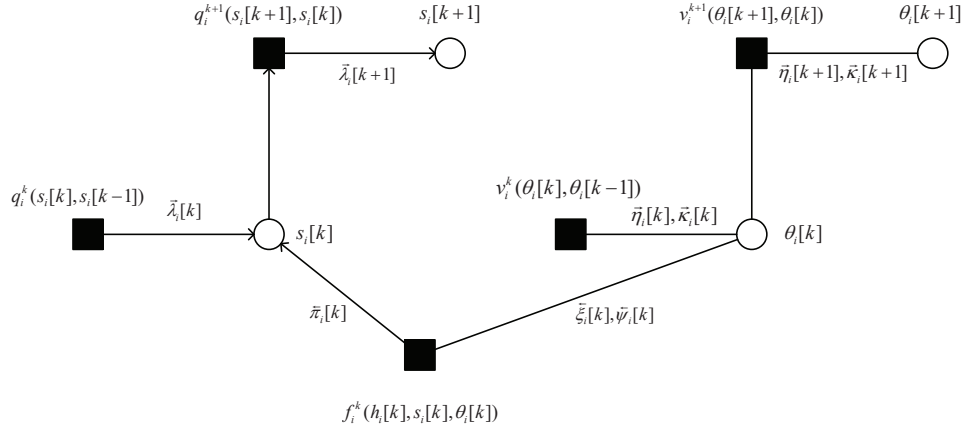


Fig. 4. factor graph for across stage

where \mathcal{A}_q^c represents the subset of \mathcal{A} consisting of the symbol for which the q^{th} bit is $c \in \{0, 1\}$.

C. Updating the a priori Coefficient of Channel

The a priori of symbols is updated by the decoder, and we use the expectation-maximization algorithm to update the a priori coefficients $\mathbf{q} = [p_{01}, \lambda, \zeta, \varrho, \rho]$ on the channel side. Details are summarized in Table III.

TABLE III
COEFFICIENTS UPDATED BY EM

$\lambda^{\text{new}} = \frac{1}{L} \sum_{i=1}^L \frac{\bar{\pi}_i[1] \lambda \bar{\lambda}_i[1]}{(1 - \bar{\pi}_i[1])(1 - \lambda)(1 - \bar{\lambda}_i[1])}$	(B1)
$p_{01}^{\text{new}} = \frac{\sum_{k=2}^K \sum_{i=1}^L E[s_i[k-1] \bar{\mathbf{y}}] - E[s_i[k-1]s_i[k] \bar{\mathbf{y}}]}{\sum_{k=2}^K \sum_{i=1}^L E[s_i[k-1] \bar{\mathbf{y}}]}$	(B2)
$\rho^{\text{new}} = \frac{1}{L(K-1)} \sum_{k=2}^K \sum_{i=1}^L \tilde{v}_i[k] + \tilde{\mu}_i[k] ^2 + \zeta ^2 - 2\Re\{\tilde{\mu}_i[k] \zeta^k\}$	(B3)
$\zeta^{\text{new}} = \frac{\sum_{k=2}^K \sum_{i=1}^L \frac{1}{\varrho \rho} (\tilde{\mu}_i[k] - (1-\varrho)\tilde{\mu}_i[k-1]) + \sum_{i=1}^L \tilde{\mu}_i[1]/\sigma^2}{L((K-1)/\rho + 1/\sigma^2)}$	(B4)
$\varrho^{\text{new}} = \frac{1}{4L(K-1)} (b - \sqrt{b^2 + 8L(K-1)c})$	(B5)
$\tilde{v}_i[k] \triangleq V[\theta_i[k] \bar{\mathbf{y}}]$	(B6)
$\tilde{\mu}_i[k] \triangleq E[\theta_i[k] \bar{\mathbf{y}}]$	(B7)
$b \triangleq \frac{2}{\rho} \sum_{k=2}^K \sum_{i=1}^L \Re\{E[\theta_i[k] \theta_i[k-1] \bar{\mathbf{y}}]\} - \Re\{(\tilde{\mu}_i[k] - \tilde{\mu}_i[k-1]) \zeta\} - \tilde{v}_i[k-1] - \tilde{\mu}_i[k-1] ^2$	(B8)
$c \triangleq \frac{2}{\rho} \sum_{k=2}^K \sum_{i=1}^L \tilde{v}_i[k] + \tilde{\mu}_i[k] ^2 + \tilde{v}_i[k-1] + \tilde{\mu}_i[k-1] ^2 - 2\Re\{E[\theta_i[k] \theta_i[k-1] \bar{\mathbf{y}}]\}$	(B9)

Herein, we complete the entire description of the DCS-BiGAMP-based joint channel estimation and equalization/decoding algorithm. We name it DCS-JCED and summarize it in Algorithm 1.

IV. NUMERICAL SIMULATION

We present the numerical results of DCS-JCED in comparison with the original JCED and classic CE-based LMMSE turbo equalizer. We evaluate the performance from multiple perspectives, including BER, NMSE of the channel under different signal-to-noise ratios (E_b/N_0), pilot-to-data rate $N_p/(N_p + N_{cd})$, time of forward propagation T_{fp} and backward propagation T_{pb} , the number of data frames K demodulated at the same time.

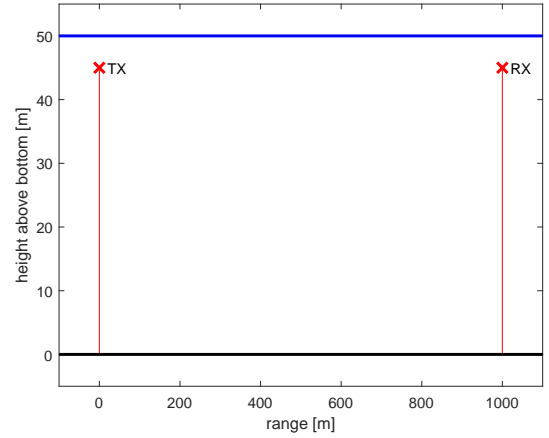


Fig. 5. UWA simulation environment.

A. Simulation Setup

To improve simulation realism, we use the UWA model proposed in [25] and its MATLAB toolbox [24]. This model has been widely accepted and verified by a large amount of sea trial data obtained by Surface Processes and Acoustic Communications Experiment (SPACE), Mobile Acoustic Communications Experiment (MAC) and Kauai AComms Multidisciplinary University Research Initiative (KAM). Here, we set the depth of the sea to 50 m and place the transmitter and receiver at a depth of 5 m with a distance of 1000 m, as shown in Fig 5. The range of the surface height variation, transmitter height variation, and receiver height variation is set between -1.25 m and 1.25 m, while the range of channel distance variation is set between -20 m and 20 m. Under these conditions, we generated 200 channel, and an example of the channel is provided in Fig. 6.

In the simulation, we set the transmission symbol rate to 4 kbit/s, which leads to a tap delay resolution of 0.25 ms, as in Fig. 6. The dominant components of the channel delay taps are concentrated within the first 6 milliseconds. Therefore, we take the first 25 taps as the true channel in our simulation. The frame structure is as follows: the length of guard sequence N_g

Algorithm 1 DCS-JCED

Input: bit *a priori* L_{apr} , channel *a priori* coefficients $\mathbf{q} = [p_{01}, \lambda, \zeta, \varrho, \rho]$, AWGN noise variance σ_w , number of forward propagation T_{fp} , number of backward propagation T_{bp} , number of inner BiGAMP iteration T_{inner} , number of turbo iteration T_{turbo} .

Initialization: $\{\hat{r}_j[k]\}_{j=1}^{N_p} = x_{p,j}$, $\{\hat{\mu}_j^r[k]\}_{j=1}^{N_p} = \epsilon$, $\{\hat{r}_j[k]\}_{j=N_p+1}^{N_p+N_{\text{cd}}+N_g} = 0$, $\{\hat{\mu}_j^r[k]\}_{j=N_p+1}^{N_p+N_{\text{cd}}} = 1$, $\{\hat{\mu}_j^r[k]\}_{j=N_p+N_{\text{cd}}+1}^{N_p+N_{\text{cd}}+N_g} = \epsilon$, $\{\hat{q}_i[k] = q_i^{\text{init}}[k]\}_{i=1}^L$, $\{\hat{\mu}^q = (\mu^q[k])^{\text{init}}\}_{i=1}^L$, $\{\hat{s}_m\}_{m=1}^M = 0$, $\epsilon \rightarrow 0$.

for $t_{\text{turbo}} = 1, \dots, T_{\text{turbo}}$ **do**
 initialize $t_{\text{fp}} = 0$, $t_{\text{bp}} = 0$.
if $t_{\text{fp}} < T_{\text{fp}}$ **do**
 $t_{\text{fp}} = t_{\text{fp}} + 1$
for $k = 1, \dots, K$ **do forward propagation**
into stage $\forall i$ calculate local prior $\vec{\pi}_i[k]$, $\vec{\xi}_i[k]$, $\vec{\psi}_i[k]$ by (14), (17), (16)
within stage
for $t_{\text{inner}} = 1, 2, \dots, T_{\text{inner}}$
step I $\forall i$ update *a posteriori* coefficients of $\hat{h}_i[k]$, $\mu_i^h[k]$ by (22), (23)
 $j \in [N_p + 1, N_p + N_{\text{cd}}]$ update *a posteriori* coefficients of $\hat{x}_j[k]$, $\mu_j^x[k]$ by (27), (28)
step II $\forall m$ update the conditional coefficients of $\mathbf{z}[k]$, i.e. $\hat{p}_m[k]$, $v_m^p[k]$ by (29), (30)
step III $\forall m$ update the *a posteriori* coefficients of $\mathbf{z}[k]$, i.e. $\hat{z}_m[k]$, $\mu_m^z[k]$ by (36), (35)
step IV $\forall m$ update the Taylor coefficients $\hat{s}_m[k]$, $\mu_m^s[k]$ by (37), (38)
step V $\forall i$ update the extrinsic coefficients of $\hat{q}_i[k]$, $\mu_i^q[k]$ by (40), (39)
 $j \in [N_p + 1, N_p + N_{\text{cd}}]$ update the extrinsic coefficients of $\hat{r}[k]$, $\mu_i^r[k]$ by (42), (41)
endfor
out stage $\forall i$ calculate $\overleftarrow{\pi}_i[k]$, $\overleftarrow{\xi}_i[k]$, $\overleftarrow{\psi}_i[k]$ by (45), Table II
forward across stage $\forall i$ calculate $\vec{\lambda}_i[k+1]$, $\vec{\eta}_i[k+1]$, $\vec{\kappa}_i[k+1]$ by (49), (52), (53)
end for
end if
if $t_{\text{bp}} < T_{\text{bp}}$ **do**
 $t_{\text{bp}} = t_{\text{bp}} + 1$
backward propagation
end if
EM tuning
 update $\mathbf{q} = [p_{01}, \lambda, \zeta, \varrho, \rho]$ by Table III
decoding
 calculate L_{ext} by (54) and send into decoder to get L_{apr}
end for

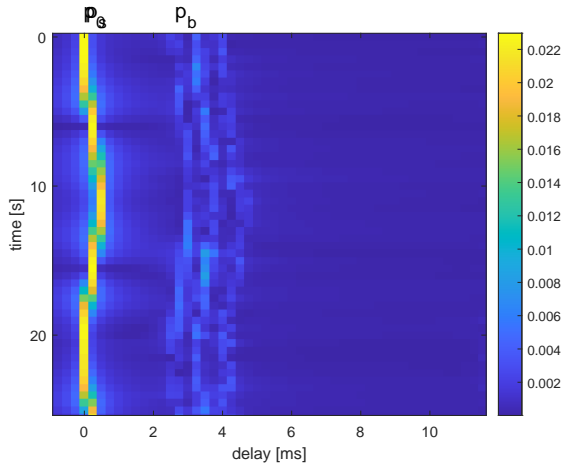


Fig. 6. Simulated channel impulse responses.

is set to 25, the pilot is an M-sequence modulated by phase shift keying (PSK), and the length of pilot N_p is selected from

31 or 63 in different simulations. $N_b = 130$ data bits are coded at a rate of 1/2 using LDPC code and then mapped to quadrature phase shift key (QPSK), resulting in $N_{\text{cd}} = 130$ data symbols per data frame. In this case, the total data frame length is selected from $N_c = 186$ or 218, such that the maximum time duration of a data frame is 0.0545 s. Given a time resolution of 0.05 s, we take one row of the simulated channel through which a data frame passes. For a transmission containing 10 data frames, one example channel is shown in Fig 7.

B. Performance analysis

We first analyze the relationship between BER, estimated channel NMSE and bit SNR E_b/N_0 . We set $N_p = 63$ and transmit 10 data frames at a time, with the forward propagation T_{fp} and T_{bf} both set to 2. We simulate 200 channels and run 200 simulations for each channel. The MMSE turbo equalizer uses the LMMSE algorithm to estimate the channel, while both JCED and DCS-JCED use a Gaussian random sequence to initialize the channel. For fairness, we use the *a posteriori* channel estimates of the k^{th} data frame to initialize the channel

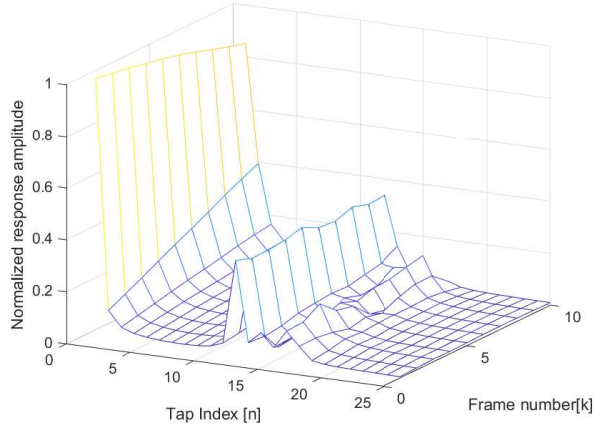


Fig. 7. Absolute-value amplitude of example channel for 10 data frames in transmission simulation.

of the $(k + 1)^{\text{th}}$ data frame when performing JCED on the $(k + 1)^{\text{th}}$ data frame. Furthermore, the number of iterations T_{inner} is 100 for JCED and 25 for DCS-JCED. For all methods, we perform turbo iteration 3 times. The lengths of the non-causal and causal parts of the filter N_1 and N_2 in the MMSE turbo equalizer [3] are set to 15 and 20, respectively. The initial parameters of the Bernoulli Gaussian distribution for DCS-JCED and JCED are set to $\lambda = 0.2$, $\zeta = 0$, $\rho = 1$. For parameters that characterize the time-varying feature of the channel, we initialize them by setting $p_{01} = 0.01$ and $\varrho = 0.005$. We set the breakout condition of the iteration $\|\hat{\mathbf{z}}^t[k] - \hat{\mathbf{z}}^{t-1}[k]\|_2 / \|\hat{\mathbf{z}}^{t-1}[k]\|_2 < 10^{-4}$, where $\hat{\mathbf{z}}^t[k]$ is the estimation of $\mathbf{z}[k]$ in the current iteration, and $\hat{\mathbf{z}}^{t-1}[k]$ is the estimation in the last iteration. The BER curves are shown in Fig. 8, and the NMSE curves of the estimated channel are shown in Fig. 9. Due to the low SNR and short pilot length, the NMSE of the LMMSE channel estimator is relatively high, resulting in poor BER performance in equalization. At this point, the turbo equalization operation impacts negatively since the results of the equalizer are no longer reliable with such a high BER. The original JCED performs well in this scenario, since it can jointly utilize the soft information of both the channel and symbols. Turbo equalization not only reduces the BER but also significantly reduces the NMSE of the channel estimates between one and two turbo iterations. Building on this groundwork, DCS-JCED utilizes the information of multiple data frames by passing messages across them, thus achieving the best BER and NMSE performance. Note that DCS-JCED reduces the NMSE of channel estimates more rapidly between one and two turbo iterations than the original JCED.

After changing the pilot number, while keeping other parameters the same, to 31, the BER and estimated channel NMSE curves in Fig. 10 and 11 show a loss of performance across all methods. The MMSE equalizer fails completely since the pilot length is too short for LMMSE channel estimator to obtain a reliable result. The NMSE of the LMMSE channel estimator is much higher than that of the original JCED and the proposed DCS-JCED. Although both the JCED and

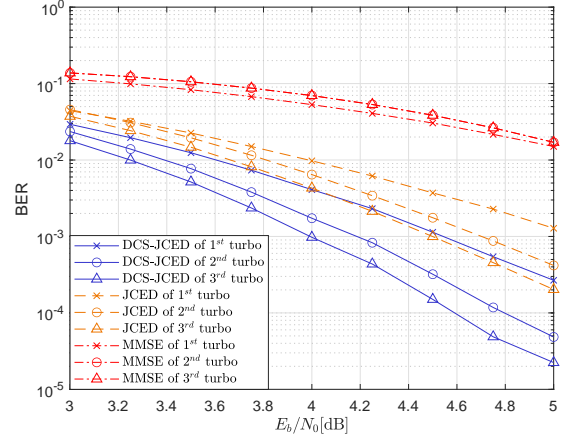


Fig. 8. BER versus E_b/N_0 for $K = 10$, $N_p = 63$, $T_{\text{ip}} = T_{\text{bp}} = 2$.

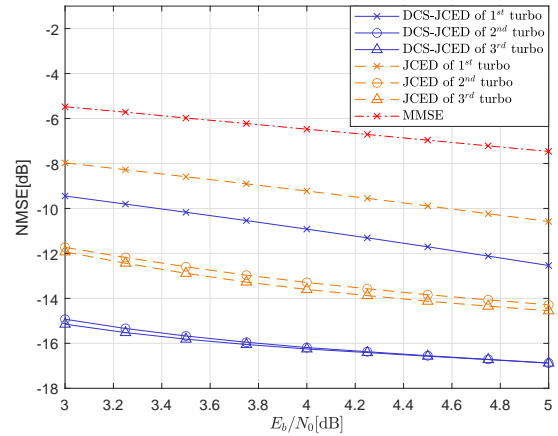


Fig. 9. Estimated channel NMSE versus E_b/N_0 for $K = 10$, $N_p = 63$, $T_{\text{ip}} = T_{\text{bp}} = 2$.

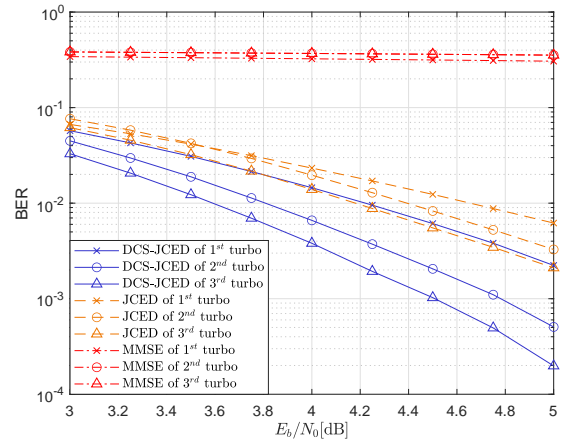


Fig. 10. BER versus E_b/N_0 for $K = 10$, $N_p = 31$, $T_{\text{ip}} = T_{\text{bp}} = 2$.

DCS-JCED suffer a performance loss, their NMSE remains at a low level, and their BER results are an order of magnitude worse compared to the results using $N_p = 63$. It should be

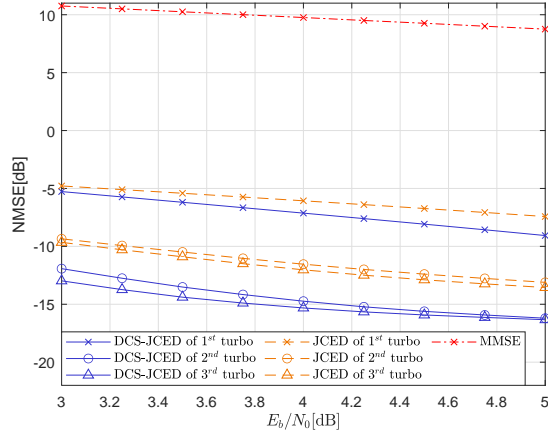


Fig. 11. Estimated channel NMSE versus E_b/N_0 for $K = 10$, $N_p = 31$, $T_{fp} = T_{bp} = 2$.

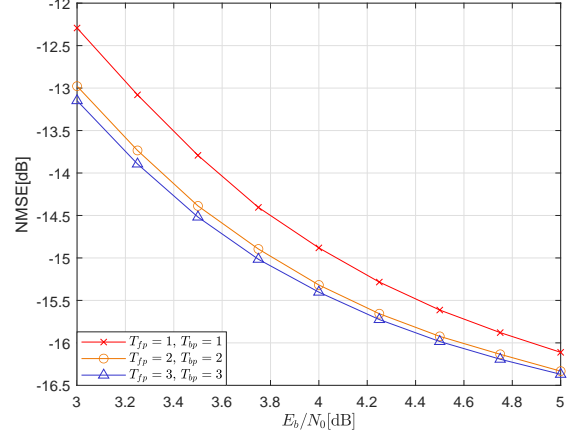


Fig. 13. Estimated channel NMSE versus E_b/N_0 of 3rd turbo iteration for $K = 10$, $N_p = 31$ and different T_{fp} , T_{bp} in DCS-JCED.

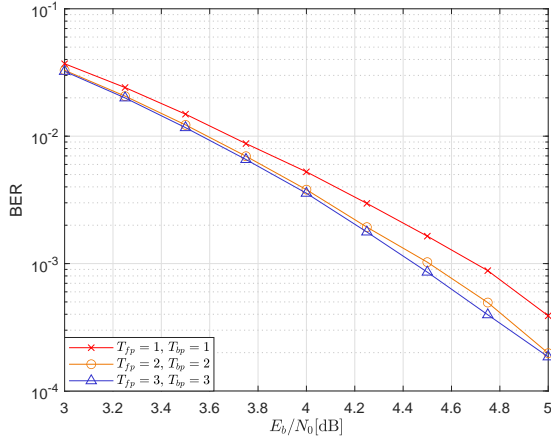


Fig. 12. BER versus E_b/N_0 of 3rd turbo iteration for $K = 10$, $N_p = 31$ and different T_{fp} , T_{bp} in DCS-JCED.

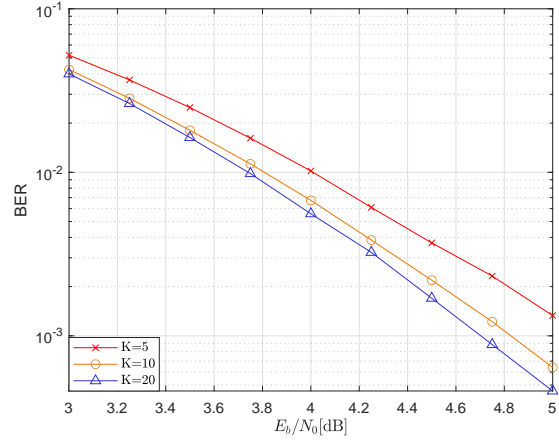


Fig. 14. BER versus E_b/N_0 of 3rd turbo iteration for $N_p = 31$, $T_{fp} = 1$, $T_{bp} = 1$ and different K in DCS-JCED.

noted that to achieve the same NMSE performance as that with $N_p = 63$, the LMMSE channel estimator requires an E_b/N_0 of approximately 20dB. At such an E_b/N_0 level, the JCED and DCS-JCED already achieve error-free transmission. When comparing the results of JCED and DCS-JCED, we observe that DCS-JCED again has the best BER and NMSE performance.

Since the proposed DCS-JCED uses both forward and backward propagation to pass messages between every data frame, we evaluate its performance with respect to the propagation time. We conduct simulations by setting 1, 2 and 3 forward and backward propagations, with $N_p = 31$, $K = 10$, and $T_{inner} = 50$. BER curves versus E_b/N_0 after 3 turbo iterations are shown in Fig. 12. It is evident that the performance of DCS-JCED gradually improves with the increased T_{fp} and T_{bp} . It can be interpreted that each data frame receives information from other data frames through *across*-stage message passing, and with an increase in the propagation times, messages passed among them becomes more reliable. However, this benefit will gradually decrease as the number of propagation

increases, since more propagations will not provide extra information for *within*-stage processing. Fig. 12 illustrates that, the performance gain between $T_{fp} = T_{bp} = 1$ and $T_{fp} = T_{bp} = 2$ is much higher than that between $T_{fp} = T_{bp} = 2$ and $T_{fp} = T_{bp} = 3$. This phenomenon can also be observed in the estimated channel NMSE curves versus E_b/N_0 as shown in Fig. 13. It is reasonable to predict that both the BER and NMSE curves versus E_b/N_0 will converge to a fixed curve with more forward and backward propagations.

The proposed DCS-JCED algorithm has the main feature of utilizing information across multiple data frames. Consequently, we analyze the performance of DCS-JCED with varying numbers of data frames in transmission. If we transmit multiple data frames, we may divide them into several groups and perform DCS-JCED on each group at the receiver. In the numerical simulation, we set the total number of transmitted data frames to 20, and at the receiver, we divide them into 4, 2 and 1 group(s) and use DCS-JCED to demodulate them, i.e. demodulating 5 data frames for 4 times, 10 data frames for 2 times and 20 data frames at once. The results of the BER

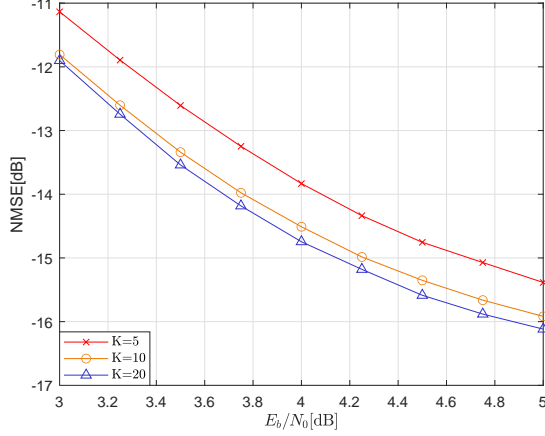


Fig. 15. Estimated channel NMSE versus E_b/N_0 of 3rd turbo for $N_p = 31$, $T_{ip} = 1$, $T_{bp} = 1$ and different K in DCS-JCED.

and estimated channel NMSE curves versus E_b/N_0 are shown in Fig. 14 and 15 respectively. As expected, the performance of DCS-JCED improves as the number of data frames being demodulated at once, i.e. K , increases. This is because each data frame exchanges information with others, and therefore, the DCS-JCED algorithm can utilize more information as the number of data frames increases. However, the performance gain generated by this effect also tends to saturate with the increase of K . One can observe that both the BER and NMSE improvement between $K = 20$ and $K = 10$ is less than that between $K = 10$ and $K = 5$, which suggests that the information exchange between different data frames reaches a limit with the increasing number of data frames.

V. CONCLUSIONS

In this paper, we propose a joint channel estimation and symbol equalization/decoding equalizer named DCS-JCED with fully soft-in and soft-out functionality. Our equalizer is based on the DCS-BiGAMP algorithm which combines the strengths of existing DCS-AMP and BiGAMP algorithms. By using DCS-JCED, we can fully utilize the soft information of both the channel and symbols across multiple data frames, whereas traditional JCED algorithm based on BiGAMP only considers information within a single data frame. The proposed equalizer can also be performed in both the time and frequency domains.

Numerical simulations conducted on a time-varying UWA channel demonstrate that the proposed algorithm outperforms the classic CE-based LMMSE equalizer and the original JCED equalizer in both the BER and estimated channel NMSE performance.

The DCS-BiGAMP algorithm employed in the equalizer design is also applicable to other bilinear compressive sensing problems that have multiple measurements vectors, such as video denoising.

APPENDIX WITHIN STAGE IN FREQUENCY DOMAIN

Here, we provide a frequency-domain version of the iteration in the *within* stage. The computational procedure for the *a posteriori* expectation and variance of $\mathbf{x}[k]$ and $\mathbf{h}[k]$ remains the same as that in the time domain. The conditional expectation and variance of $\mathbf{z}[k]$ in the frequency domain, $\bar{\mathbf{z}}[k] = \mathbf{F}_M \mathbf{z}[k] / \sqrt{M}$, are

$$\mathbf{v}^p[k] = \bar{\mathbf{v}}^p[k] + \left(\frac{1}{M} \sum_{j=1}^M \mu_j^x[k] \right) \left(\frac{1}{M} \sum_{l=1}^L \mu_l^h[k] \right) \mathbf{1}_M \quad (55)$$

$$\hat{\mathbf{p}}[k] = (\mathbf{F}_M \hat{\mathbf{x}}[k]) \odot (\mathbf{F}_M^{1:L} \hat{\mathbf{h}}[k]) - \hat{\mathbf{s}}[k] \odot \bar{\mathbf{v}}^p[k], \quad (56)$$

where

$$\begin{aligned} \bar{\mathbf{v}}^p[k] &= \frac{1}{M} \sum_{j=1}^M \mu_j^x[k] \left| \mathbf{F}_M^{1:L} \hat{\mathbf{h}}[k] \right|^{\odot 2} \\ &+ \frac{1}{M} \sum_{l=1}^L \mu_l^h[k] \left| \mathbf{F}_M \hat{\mathbf{x}}[k] \right|^{\odot 2}. \end{aligned} \quad (57)$$

$\hat{\mathbf{s}}[k]$ and $\boldsymbol{\mu}^s[k]$ are the same as those in the time-domain version. To calculate the extrinsic parameters of $\mathbf{x}[k]$ and $\mathbf{h}[k]$, we have

$$\begin{aligned} \boldsymbol{\mu}^r[k] &= M / \left((\boldsymbol{\mu}^s[k])^T \left| \mathbf{F}_M^{1:L} \hat{\mathbf{h}}[k] \right|^{\odot 2} \right) \mathbf{1}_L \\ &= \mu^r[k] \mathbf{1}_L \end{aligned} \quad (58)$$

$$\begin{aligned} \boldsymbol{\mu}^q[k] &= M / \left((\boldsymbol{\mu}^s[k])^T \left| \mathbf{F}_M \hat{\mathbf{x}}[k] \right|^{\odot 2} \right) \mathbf{1}_M \\ &= \mu^q[k] \mathbf{1}_M \end{aligned} \quad (59)$$

and

$$\begin{aligned} \hat{\mathbf{r}}[k] &= \hat{\mathbf{x}}[k] + \mu^r[k] \mathbf{F}_M^H \left((\mathbf{F}_M^{1:L} \hat{\mathbf{h}}[k])^* \odot \hat{\mathbf{s}}[k] \right) \\ &- \mu^s[k] \mu^r[k] \mu^h[k] \hat{\mathbf{x}}[k] \end{aligned} \quad (60)$$

$$\begin{aligned} \hat{\mathbf{q}}[k] &= \hat{\mathbf{h}}[k] + \mu^q[k] \mathbf{F}_M^{1:L H} \left((\mathbf{F}_M \hat{\mathbf{x}}[k])^* \odot \hat{\mathbf{s}}[k] \right) \\ &- \mu^s[k] \mu^q[k] \mu^x[k] \hat{\mathbf{h}}[k], \end{aligned} \quad (61)$$

where

$$\boldsymbol{\mu}^s[k] = \frac{1}{M} \sum_{m=1}^M \mu_m^s[k] \quad (62)$$

$$\mu_h[k] = \frac{1}{L} \sum_{l=1}^L \mu_l^h[k] \quad (63)$$

$$\mu^x[k] = \frac{1}{M} \sum_{j=1}^M \mu_j^x[k]. \quad (64)$$

REFERENCES

- [1] G. K. Kaleh, "Channel equalization for block transmission systems," *IEEE J. Sel. Areas Commun.*, vol. 13, no. 1, pp. 110–121, 1995.
- [2] S. Zhou and Z. Wang, *OFDM for underwater acoustic communications*. John Wiley & Sons, 2014.
- [3] M. Tuchler, A. Singer, and R. Koetter, "Minimum mean squared error equalization using a priori information," *IEEE Trans. Signal Process.*, vol. 50, no. 3, pp. 673–683, 2002.
- [4] Q. Guo, D. Huang, S. Nordholm, J. Xi, and Y. Yu, "Iterative frequency domain equalization with generalized approximate message passing," *IEEE Signal Process. Lett.*, vol. 20, no. 6, pp. 559–562, 2013.
- [5] M. Gong, F. Chen, H. Yu, Z. Lu, and L. Hu, "Normalized adaptive channel equalizer based on minimal symbol-error-rate," *IEEE Trans. Commun.*, vol. 61, no. 4, pp. 1374–1383, 2013.
- [6] J. Xi, S. Yan, L. Xu, and C. Hou, "Sparsity-aware adaptive turbo equalization for underwater acoustic communications in the mariana trench," *IEEE J. Ocean. Eng.*, vol. 46, no. 1, pp. 338–351, 2020.
- [7] J. Hao, J. Wang, Y. R. Zheng, and J. Song, "MIMO TDS-OFDM for underwater acoustic communication with turbo equalization," in *Proc. OCEANS 2015 - MTS/IEEE WASHINGTON*, 2015, pp. 1–6.
- [8] M. Reuter, J. Allen, J. Zeidler, and R. North, "Mitigating error propagation effects in a decision feedback equalizer," *IEEE Trans. Commun.*, vol. 49, no. 11, pp. 2028–2041, 2001.
- [9] J. T. Parker and P. Schniter, "Parametric bilinear generalized approximate message passing," *IEEE J. Sel. Topics Signal Process.*, vol. 10, no. 4, pp. 795–808, 2016.
- [10] P. Sun, Z. Wang, and P. Schniter, "Joint channel-estimation and equalization of single-carrier systems via bilinear amp," *IEEE Trans. Signal Process.*, vol. 66, no. 10, pp. 2772–2785, 2018.
- [11] F. Kschischang, B. Frey, and H.-A. Loeliger, "Factor graphs and the sum-product algorithm," *IEEE Trans. Inf. Theory*, vol. 47, no. 2, pp. 498–519, 2001.
- [12] X. Qin and R. Diamant, "Joint channel estimation and decoding for underwater acoustic communication with a short pilot sequence," *IEEE J. Ocean. Eng.*, 2023.
- [13] J. Yang, X. Yuan, X. Liao, P. Llull, D. J. Brady, G. Sapiro, and L. Carin, "Video compressive sensing using gaussian mixture models," *IEEE Trans. Image Process.*, vol. 23, no. 11, pp. 4863–4878, 2014.
- [14] W. Li and J. C. Preisig, "Estimation of rapidly time-varying sparse channels," *IEEE J. Ocean. Eng.*, vol. 32, no. 4, pp. 927–939, 2007.
- [15] D. Angelosante, G. B. Giannakis, and E. Grossi, "Compressed sensing of time-varying signals," in *Proc. Int. Conf. Digital Signal Process.*, 2009, pp. 1–8.
- [16] W. Dai, D. Sejdinovic, and O. Milenkovic, "Gaussian dynamic compressive sensing," in *Int'l Conf. on Sampling Theory and Appl. (SampTA)*, 2011.
- [17] Z. Zhang and B. D. Rao, "Sparse signal recovery with temporally correlated source vectors using sparse bayesian learning," *IEEE J. Sel. Topics Signal Process.*, vol. 5, no. 5, pp. 912–926, 2011.
- [18] J. Ziniel and P. Schniter, "Dynamic compressive sensing of time-varying signals via approximate message passing," *IEEE Trans. Signal Process.*, vol. 61, no. 21, pp. 5270–5284, 2013.
- [19] D. Wipf, "Sparse estimation with structured dictionaries," in *Proc. Adv. Neural Inf. Process. Syst.*, 2011, pp. 2016–2024.
- [20] R. Koetter, A. C. Singer, and M. Tuchler, "Turbo equalization," *IEEE Signal Process. Mag.*, vol. 21, no. 1, pp. 67–80, 2004.
- [21] J. S. Yedidia, W. T. Freeman, and Y. Weiss, "Understanding belief propagation and its generalizations," in *Exploring artificial intelligence in the new millennium*, 2003, pp. 239–269.
- [22] L. Bahl, J. Cocke, F. Jelinek, and J. Raviv, "Optimal decoding of linear codes for minimizing symbol error rate (corresp.)," *IEEE Trans. Inf. Theory*, vol. 20, no. 2, pp. 284–287, 1974.
- [23] Y. Li, B. Vucetic, and Y. Sato, "Optimum soft-output detection for channels with intersymbol interference," *IEEE Trans. Inf. Theory*, vol. 41, no. 3, pp. 704–713, 1995.
- [24] P. Qarabaqi and M. Stojanovic, "Acoustic channel simulator," 2013. [Online]. Available: <http://millitsa.coe.neu.edu/projects.html>
- [25] —, "Statistical characterization and computationally efficient modeling of a class of underwater acoustic communication channels," *IEEE J. Ocean. Eng.*, vol. 38, no. 4, pp. 701–717, 2013.
- [26] H.-A. Loeliger, "An introduction to factor graphs," *IEEE Signal Process. Mag.*, vol. 21, no. 1, pp. 28–41, 2004.
- [27] S.-Y. Chung, T. Richardson, and R. Urbanke, "Analysis of sum-product decoding of low-density parity-check codes using a gaussian approximation," *IEEE Trans. Inf. Theory*, vol. 47, no. 2, pp. 657–670, 2001.
- [28] J. P. Vila and P. Schniter, "Expectation-maximization gaussian-mixture approximate message passing," *IEEE Trans. Signal Process.*, vol. 61, no. 19, pp. 4658–4672, 2013.
- [29] S. Rangan, P. Schniter, and A. K. Fletcher, "Vector approximate message passing," *IEEE Trans. Inf. Theory*, vol. 65, no. 10, pp. 6664–6684, 2019.
- [30] P. Bromiley, "Products and convolutions of gaussian probability density functions," *Tina-Vision Memo*, vol. 3, no. 4, p. 1, 2003.
- [31] J. Ziniel and P. Schniter, "Efficient high-dimensional inference in the multiple measurement vector problem," *IEEE Trans. Signal Process.*, vol. 61, no. 2, pp. 340–354, 2013.
- [32] M. Tüchler and A. C. Singer, "Turbo equalization: An overview," *IEEE Trans. Inf. Theory*, vol. 57, no. 2, pp. 920–952, 2011.
- [33] C. Laot, A. Glavieux, and J. Labat, "Turbo equalization: adaptive equalization and channel decoding jointly optimized," *IEEE J. Sel. Areas Commun.*, vol. 19, no. 9, pp. 1744–1752, 2001.